Nanotechnology **21** (2010) 415301 (7pp) doi:10.1088/0957-4484/21/41/415301

# Surface-enhanced Raman nanodomes

**Charles J Choi[1], Zhida Xu[1], Hsin-Yu Wu[1], Gang Logan Liu[1] and Brian T Cunningham[1,2]**

[1] Department of Electrical and Computer Engineering, Micro and Nanotechnology Laboratory, University of Illinois at Urbana-Champaign, 208 North Wright Street, Urbana, IL 61801, USA
[2] Department of Bioengineering, Micro and Nanotechnology Laboratory, University of Illinois at Urbana-Champaign, 208 North Wright Street, Urbana, IL 61801, USA

E-mail: bcunning@illinois.edu

Received 10 June 2010, in final form 8 August 2010
Published 13 September 2010
Online at stacks.iop.org/Nano/21/415301

**Abstract**

We demonstrate a surface-enhanced Raman scattering (SERS) substrate consisting of a closely spaced metal nanodome array fabricated on flexible plastic film. We used a low-cost, large-area replica molding process to produce a two-dimensional periodic array of cylinders that is subsequently overcoated with $SiO_2$ and silver thin films to form dome-shaped structures. Finite element modeling was used to investigate the electromagnetic field distribution of the nanodome array structure and the effect of the nanodome separation distance on the electromagnetic field enhancement. The SERS enhancement from the nanodome array substrates was experimentally verified using rhodamine 6G as the analyte. With a separation distance of 17 nm achieved between adjacent domes using a process that is precisely controlled during thin film deposition, a reproducible SERS enhancement factor of $1.37 \times 10^8$ was demonstrated. The nanoreplica molding process presented in this work allows for simple, low-cost, high-throughput fabrication of uniform nanoscale SERS substrates over large surface areas without the requirement for high resolution lithography or defect-free deposition of spherical microparticle monolayer templates.

(Some figures in this article are in colour only in the electronic version)

## 1. Introduction

Due to its capability for specific chemical identification through measurement of vibrational energies associated with chemical bonds in molecules, Raman spectroscopy is a powerful and versatile method for label-free molecular identification. As a general purpose analytical method, the applications for Raman spectroscopy span a broad range of fields that includes protein–protein interaction analysis, DNA/RNA hybridization, aptamer conformational change, viral particle detection, bacteria identification, and detection of explosives [1–6]. As first observed and theoretically understood, the extremely small Raman scattering cross section may be enhanced when a molecule is in close proximity to a roughened metal surface that supports regions of heightened electromagnetic field intensity [7, 8]. The first demonstrated surface-enhanced Raman spectroscopy (SERS) substrates, providing enhancement factors of $\sim 10^6$, were made from electrochemically roughened silver electrodes produced by repeated oxidation–reduction cycles [7–9]. The SERS enhancement enables Raman scattering spectra to be gathered rapidly with substantially less laser power, resulting in many detection applications becoming more feasible, provided that the analytes have an opportunity to come into contact with the SERS-active surface.

In recent years, with advancements in nanofabrication technology and the broad availability of computer simulation tools that enable investigation of the interactions of metal/dielectric nanostructures with electromagnetic fields, a wide variety of nanoparticle shapes and structures have been demonstrated as SERS-active surfaces with greater enhancement factors. For example, colloidal metal (silver or gold) nanoparticle clusters of 100–150 nm diameter, dispersed in solution have been used to achieve single-molecule SERS detection, with reported enhancement factors as high as $\sim 10^{15}$ [10, 11]. Nanoparticles with sharp tips, such as metallic 'nanocrescents' have demonstrated enhancement factors of $>10^{10}$ through the effects of electromagnetic field focusing into a small volume when the particle couples with an externally applied laser source through surface plasmons [12]. While SERS approaches using colloidal metal aggregates can produce large enhancement factors, their use is limited due to the lack of enhancement factor reproducibility and low overall 'hot spot' volume density stemming from their sensitivity to random nanocluster morphology [13, 14].

 

Compared to SERS-active nanoparticles suspended in solution, SERS-active surfaces can be fabricated with engineered three-dimensional topologies using a wide variety of lithography approaches to precisely define desired features. SERS surfaces are especially desirable in applications for which one wishes to measure Raman spectra without adding nanoparticles to a test sample, and for multiplexed arrays of Raman measurements. For example, using electron-beam lithography to fabricate uniform, closely spaced circular, triangle, and square shaped metal nanoparticle arrays with interparticle spacing of 75–250 nm, reproducible SERS enhancement factors of $\sim 10^6$ have been demonstrated [15–18]. Recently, electron-beam lithography patterning of arrays of 200 nm diameter gold nanocylinders has been combined with gold chemical reduction to create 'plasmonic nanogalaxy' substrates that exhibit a cascade enhancement effect to generate a spatially averaged SERS enhancement factor up to $\sim 10^8$ [19]. Although large enhancement factors can be achieved using the high resolution capabilities of electron-beam lithography, the applications of such devices are limited due to the time (and associated cost) of producing such structures over surface areas greater than a few square millimeters. For this reason, there has been intense research interest in the development of processes for creating SERS substrates with a high density of electromagnetic hot spots using procedures that are more amenable to low-cost and large-area fabrication. For example, soft lithography has been used to fabricate SERS plasmonic crystals with $\sim 20 \times 20$ mm$^2$ area with an enhancement factor of $10^5$, and nanowell structures on a 4 inch diameter wafer with an enhancement factor of $10^7$ [20, 21]. Likewise, nanosphere lithography (NSL) and metal film over nanosphere (MFON) structures are effective SERS substrates in which arrays of metal triangles (for NSL) or metal domes in a periodic hexagonal lattice (for MFON) are created by deposition of metal thin films over a monolayer or multilayer of close-packed polymer or silica spheres [22–24]. MFON structures have demonstrated SERS enhancement factors of up to $10^7$ on substrates with diameter reported as large as 18 mm [25, 26]. Uniform patterning of the MFON surface is dependent upon the ability to produce a defect-free monolayer of $\sim$500–600 nm diameter polymer or silica spheres using processes such as drop coating, spin casting or controlled withdrawal of the substrate from a liquid bath.

Nanoreplica molding has been demonstrated as a low-cost method for manufacturing periodic surface structures for a variety of applications. The method is performed using low force at room temperature to produce nanometer-scale structures with high uniformity over a large surface area using a patterned silicon wafer as a reusable molding template. The area of nanoreplica molded surfaces is ultimately limited only by the size of the silicon wafer. However, the process has been adapted for fabrication upon continuous sheets of flexible plastic film in a roll-to-roll process that is capable of producing nanostructured surfaces on the scale of square meters [27]. Nanoreplica molding has been demonstrated for a variety of devices, including photonic crystal label-free biosensor microplates [28, 29], photonic crystal enhanced fluorescence microscope slides [30, 31], distributed-feedback laser biosensors [32], tunable optical filters [33], scaffolds for cartilage engineering [34], microplasma displays [35], and microfluidic channels [36–38]. In this work, we report on the demonstration of a SERS-active substrate comprised of a close-packed array of $\sim$311–377 nm diameter dome structures, fabricated by a process that combines nanoreplica molding and unpatterned blanket deposition of $SiO_2$ and Ag thin films. The thin film deposition process is used to control the spacing between adjacent domes with nanometer-scale precision to provide a uniformly distributed array of SERS hot spots that can be produced over a large surface area. An enhancement factor of $1.37 \times 10^8$ is demonstrated within the hot spot regions, resulting in an enhancement factor of $3.16 \times 10^6$ when the enhancement is averaged over the entire available surface area.

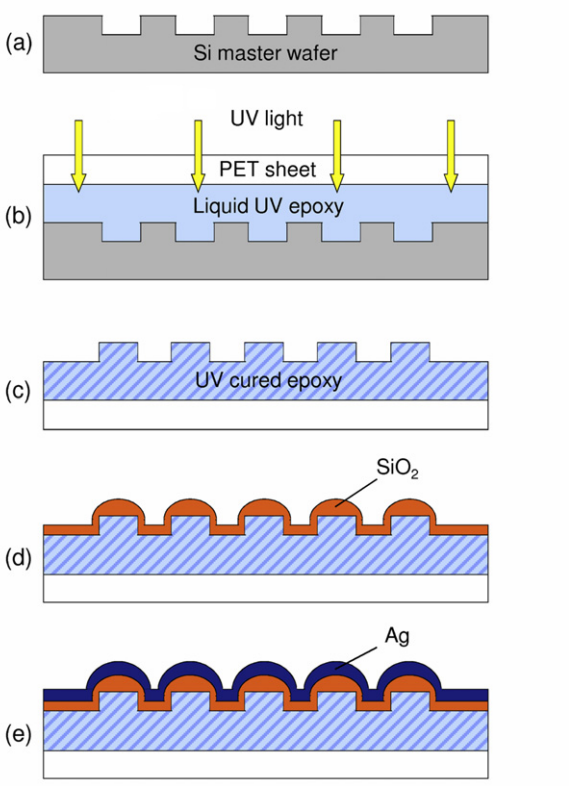


**Figure 1.** Cross section diagram of the nanoreplica molding process. (a) Fabrication of silicon master wafer template with 400 nm period 2D circular hole structure using nanoimprint lithography and reactive ion etching to a depth of 130 nm. (b) Distribution of liquid-state UV curable polymer between the silicon master wafer and the PET substrate with subsequent solidification by UV light exposure. (c) Release of the PET substrate, resulting in a polymer replica of the silicon wafer structure adhered to the PET sheet. (d)–(e) Deposition of $SiO_2$ followed by Ag on the replicated surface using electron-beam evaporation.

## 2. Nanoreplica molding process

A process flow diagram is shown in figure 1. First, nanoimprint lithography (Molecular Imprints) and reactive ion etching were used to pattern an 8 inch (200 mm) diameter silicon wafer with

a two-dimensional array of 300 nm diameter holes (period = 400 nm, depth = 130 nm), in 8 × 8 mm$^2$ dies to produce a mold template with overall feature dimensions of 120 × 120 mm$^2$ (figure 1(a)). The completed silicon mold template was subsequently immersed in dimethyl dichlorosilane (GE Healthcare) solution for 5 min followed by ethanol and DI water rinse. This treatment creates a hydrophobic silane layer on the silicon template surface which prevents cured polymer replica from adhering and therefore promotes clean release of the replica. Next, a negative volume image of the silicon surface structure was formed by pipetting liquid UV curable acrylate modified silicone polymer droplets with curing spectral range of 250–364 nm (Gelest Inc.) on the silicon wafer, placing a 250 $\mu$m thick flexible polyethylene terephthalate (PET) sheet on top, and using a Teflon roller to distribute the liquid polymer layer between the silicon wafer and the PET substrate. The liquid polymer which conformed to the shape of the features on the wafer was subsequently cured to a solid state by scanning UV light exposure throughout the entire surface for 90 s using a linear motion stage to translate the wafer. A high intensity pulsed UV curing system (Xenon Inc.) with spectral cutoff at 240 nm, peak power density of 405 W cm$^{-2}$, pulse repetition rate of 120 Hz, and pulse width of 25 $\mu$s was used (figure 1(b)). After curing, the molded structure was released from the wafer by peeling away the PET, resulting in a polymer replica of the silicon wafer structure adhered to the PET sheet (figure 1(c)). The replica molding process results in the formation of a rectangular array of ∼130 nm tall polymer cylinders that are separated by ∼100 nm at their outer perimeters. In order to produce a SERS-active surface with metal nanostructures that are separated by distances smaller than 100 nm, $SiO_2$ was applied over the polymer cylinders by electron-beam evaporation (figure 1(d)). Through control of the deposited $SiO_2$ thickness ($SiO_2$ films of 0, 50, 75, 100, and 125 nm were investigated), the cylindrical polymer surface evolves into a dome structure with a radius that increases with $SiO_2$ thickness. $SiO_2$ deposition is followed by application of a 200 nm silver thin film by electron-beam evaporation to complete the device (figure 1(e)). Figure 2 shows the image of the completed SERS nanodome array substrates fabricated on flexible PET sheets, cut into 70 × 100 mm$^2$ area. The nanoreplica molding process was performed over an area of 120 × 120 mm$^2$.

The $SiO_2$ thickness was used to control the nanodome separation distance, which is the most important variable for determination of the SERS enhancement factor. Scanning electron microscope (SEM) images of the fabricated SERS substrates are shown in figure 3. The SEM images (top view) were used to measure the minimum separation distance between adjacent domes from the base, resulting in the relationship shown in figure 4. For $SiO_2$ thicknesses of 0, 50, 75, and 100 nm, the separation distances for the nanodome arrays were 84, 59, 33, and 17 nm with the nanodome base diameters of 311, 344, 363, and 377 nm, respectively. We found that when the $SiO_2$ thickness exceeded 100 nm, the dome spacing reduced to zero, resulting in domes that touch each other, as shown in figure 3(e). SEM measurements confirmed that the replica molded structures have a period of ∼400 nm, as would be predicted by the period of the silicon mold template.

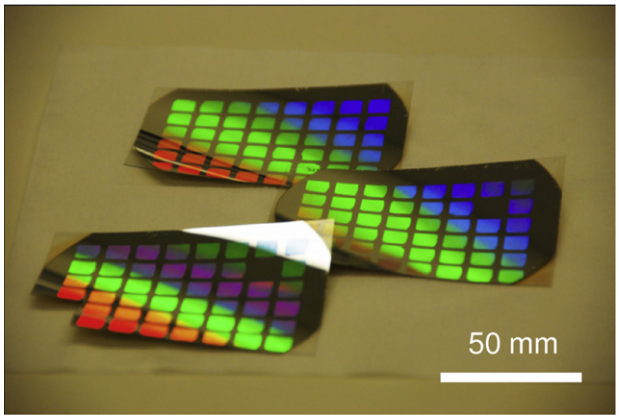


**Figure 2.** Image of the completed SERS nanodome array substrates fabricated on flexible PET sheets, cut into 70 × 100 mm$^2$ area. The nanoreplica molding process was performed over an area of 120 × 120 mm$^2$.

## 3. Computational analysis of field distribution and Raman enhancement

Since the discovery of the SERS phenomenon, the main enhancement mechanisms which have been proposed are the electromagnetic enhancement effect, the chemical enhancement effect, and enhancement of the photonic density of states [9, 39, 40]. It is generally agreed that the SERS enhancement can be approximated by the electromagnetic mechanism due to the enhanced electromagnetic fields originating from the localized surface plasmon resonance (LSPR) effect on both the incident laser and the Raman scattered radiation frequency from the analyte molecules on metal nanostructures. Such theoretical SERS enhancement has been described by the following expression [17, 41, 42]

$$\mathrm{EF_{SERS}} \propto \frac{|E_{\mathrm{loc}}(\omega_{\mathrm{ex}})|^2}{|E_0(\omega_{\mathrm{ex}})|^2}\frac{|E_{\mathrm{loc}}(\omega_{\mathrm{s}})|^2}{|E_0(\omega_{\mathrm{s}})|^2} \quad (1)$$

where $E_{\mathrm{loc}}(\omega_{\mathrm{ex}})$ is the amplitude of the enhanced local electric field at the laser excitation frequency, $E_0(\omega_{\mathrm{ex}})$ is the amplitude of the incident electric field (provided by the laser) at the laser excitation frequency, $E_{\mathrm{loc}}(\omega_{\mathrm{s}})$ is the amplitude of the enhanced local electric field at the Raman scattered frequency, and $E_0(\omega_{\mathrm{s}})$ is the amplitude of the electric field at the Raman scattered frequency (radiated by the analyte molecules).

In order to investigate the characteristics of the nanodome array structure as a SERS substrate and to study the effect of inter-dome separation distance on the SERS enhancement described by equation (1), finite element method (FEM) modeling using a commercially available software package (COMSOL Multiphysics) was utilized to map the electric field distribution around the nanodomes. The result of the 3D simulation of the electric field distribution between two adjacent nanodomes within the array is shown in figure 5(a) with the scale bar on the right side representing the normalized

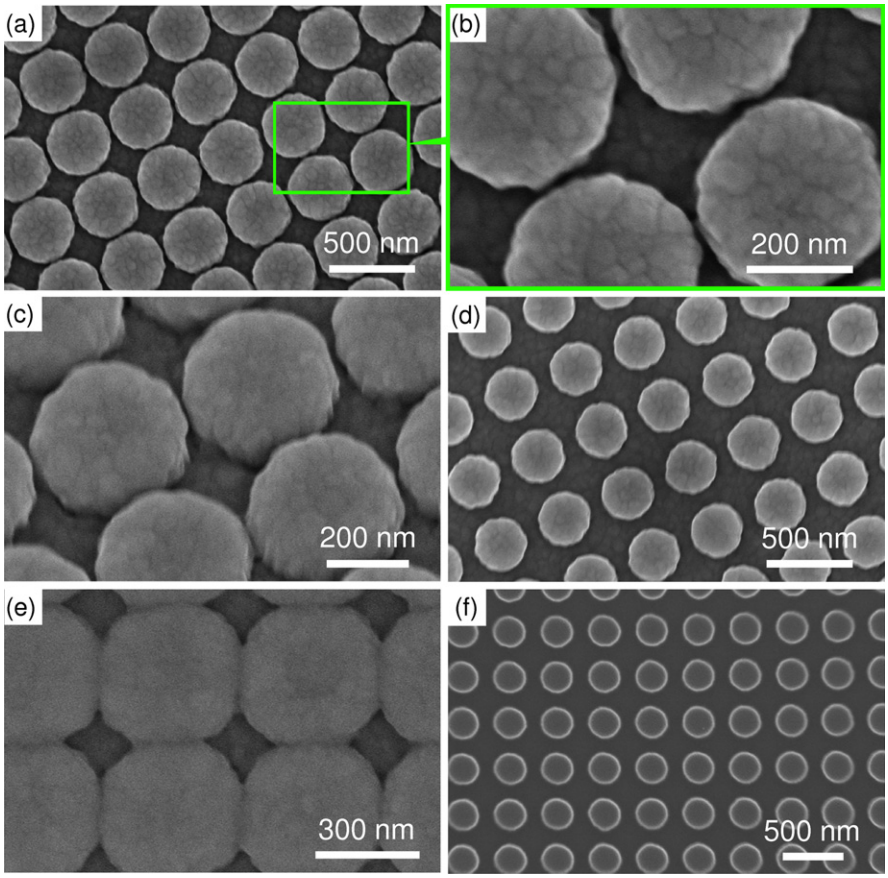


**Figure 3.** SEM images of nanodome array substrates. (a) Ag coated nanodome array substrate with measured dome separation distance of 17 nm. (b) Close-up view of the nanodome array in (a). (c) Tilted view of nanodome array substrate in (a) and (b). (d) Ag coated nanodome array substrate with measured dome separation distance of 84 nm. (e) Ag coated nanodome array substrate with domes touching each other. (f) UV cured polymer replica before $SiO_2$ and Ag deposition.

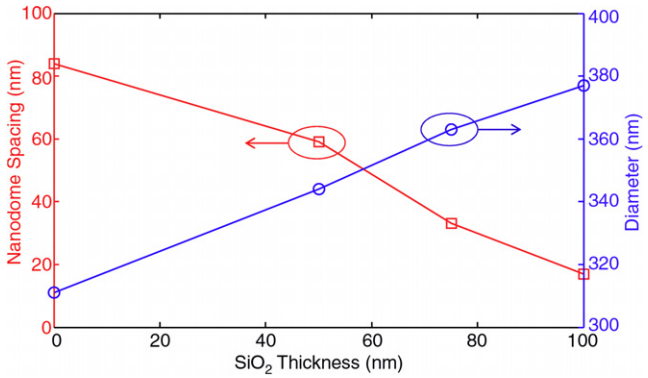


**Figure 4.** Plot of the measured nanodome separation distance (red squares, left axis) and diameter (blue circles, right axis) as a function of $SiO_2$ thickness deposited on the replica.

amplitude of the scattered electric field with respect to the incident electric field amplitude. The regions of enhanced electric field are clearly visible in the area between adjacent nanodomes where the separation distance is minimum, as expected due to the coupling effect of LSPR field enhancement. To approximate the conditions in our measurement apparatus, the nanodome arrays in the simulation were excited with a normally incident plane wave at $\lambda = 785$ nm, propagating in the $-z$ direction with linear polarization in the $x$ direction. The simulation was performed by approximating the metal-coated nanodome structure as a hemisphere. The nanodome array was modeled as a dimer structure with symmetric boundary conditions on the sidewalls of the simulation boundary, in order to reduce the computational load. Figure 5(b) shows the maximum values of Raman enhancement calculated using equation (1) from the FEM modeled electric field distribution for the laser excitation and the Raman scattered wavelength corresponding to a wavenumber shift of $\sim$1370 $cm^{-1}$ for nanodome arrays of inter-dome separation distances of 17, 33, 59, and 84 nm, to match the spacings measured by SEM.

## 4. Experimental SERS measurement

In order to experimentally verify the effect of nanodome spacing on SERS intensity, 1 $\mu$M rhodamine 6G (R6G) solution was applied to each substrate. The Raman measurement was performed using a 30 mW laser operating at $\lambda = 785$ nm, which was focused on the substrate surface by a 10$\times$ objective lens (NA = 0.28), resulting in a probe spot radius of 10 $\mu$m. SERS photons were collected by the same objective lens, into a spectrometer (Princeton Instruments) comprised of a SP2300i monochromator and a PIXIS 400 CCD (1340 $\times$ 400 pixel array) using an integration time of 1 s. The collected SERS signals were

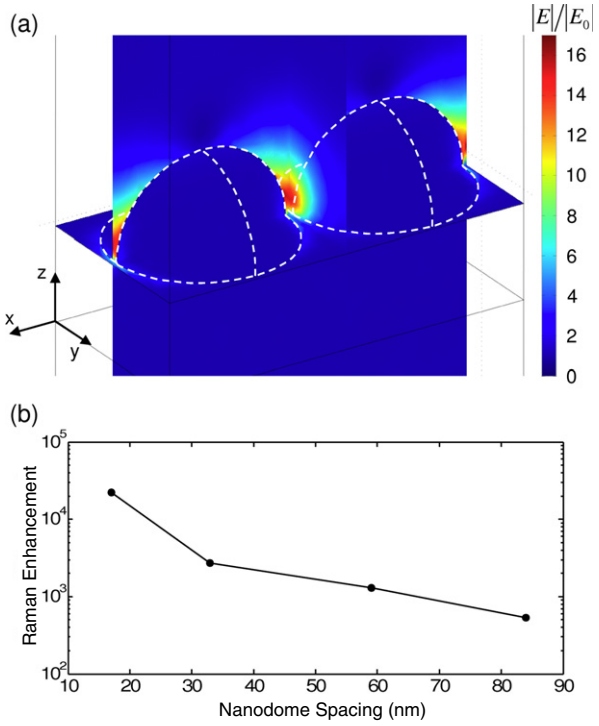


**Figure 5.** (a) 3D FEM simulation of the electric field distribution around the Ag nanodomes. The scale bar on the right side represents the normalized amplitude of the scattered electric field with respect to the incident electric field amplitude. The nanodome arrays were excited with an incident plane wave at 785 nm, propagating in the $-z$ direction with linear polarization in the $x$ direction. The nanodome array was modeled as a dimer structure with symmetric boundary conditions on the sidewalls of the simulation boundary. (b) Maximum Raman enhancement calculated from the FEM simulation of electric field distribution around the nanodome array for the laser excitation ($\lambda = 785$ nm) and the Raman scattered wavelength corresponding to wavenumber shift of $\sim$1370 cm$^{-1}$ for inter-dome separation distances of 17, 33, 59, and 84 nm.

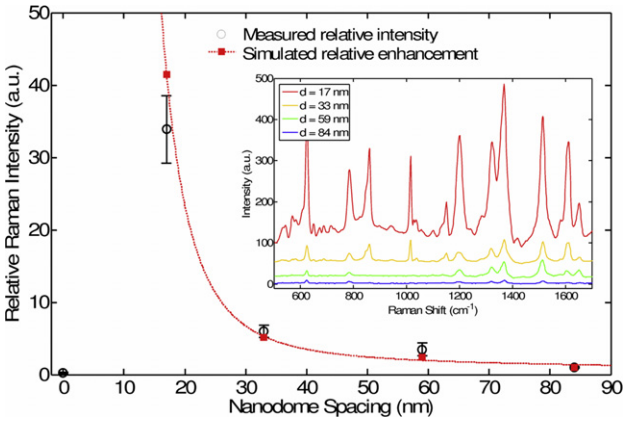


**Figure 6.** Plot of relative SERS intensity ($I(d)/I(d_{\max} = 84$ nm)) as a function of nanodome separation distance, $d$, for 1 $\mu$M R6G, measured at the Raman peak corresponding to a 1370 cm$^{-1}$ wavenumber shift. Experimentally measured relative SERS intensities are marked as black hollow dots with error bars representing $\pm 1$ standard deviation for five measurement locations throughout the nanodome array substrates for each dome separation distance ($n = 5$). Relative SERS enhancement values obtained from the FEM simulation are plotted as red squares. The inset shows example SERS spectra for the nanodome array substrates with nanodome spacings ranging from 17 to 84 nm.

processed using a multi-polynomial fitting method to remove background, and a Butterworth low-pass filter to remove noise [43]. Figure 6 shows the experimentally measured relative SERS intensity, defined as $I(d)/I(d_{\max})$ where $d_{\max} = 84$ nm, of the substrates as a function of nanodome separation distance $d$ plotted as black hollow dots. The SERS intensity values were measured at a Raman peak corresponding to a wavenumber shift of 1370 cm$^{-1}$. The error bars in the figure represent $\pm 1$ standard deviation of the relative intensity obtained for five measurement locations throughout the nanodome array substrates for each inter-dome separation distance. Figure 6 also shows the FEM-simulated relative SERS enhancement values with respect to the nanodome spacing marked as red squares. As shown in figure 6, SERS intensity/enhancement dependence on inter-dome spacing shows a very good agreement between the experimentally measured and simulated values. The inset in the figure shows example SERS spectra for devices with different separation distances ranging from 17 to 84 nm. The SERS intensity observed from the experiment demonstrates that SERS enhancement is very sensitive to inter-dome spacing, and suggests that even higher enhancements may be achievable by controlling the spacing below 17 nm. Interestingly, when adjacent nanodomes are allowed to touch each other ($d = 0$ nm), the enhancement abruptly drops down to the same value obtained when the inter-dome spacing is large. This suggests that the majority of the enhancement comes from the 'hot spot' region located in the volume between adjacent nanodomes with enhanced electromagnetic field intensity from inter-dome near-field interaction, consistent with the electric field distribution obtained from the FEM model.

## 5. SERS enhancement factor measurement

In order to experimentally measure the SERS enhancement factor for the nanodome array substrates, a concentration series of R6G molecules (1 nM–10 $\mu$M) were deposited on a SERS sensor surface with an inter-dome separation distance of $d = 17$ nm. 1 mM R6G was also deposited on the same substrate in the area outside of the nanodome region to serve as a reference. Using the same detection instrumentation and measurement parameters outlined previously, the SERS spectra shown in figure 7 were obtained.

The experimentally measured enhancement factor (EF) for a SERS system is given as [42]

$$\mathrm{EF}_{\mathrm{SERS}} = \frac{I_{\mathrm{SERS}}/N_{\mathrm{surf}}}{I_{\mathrm{ref}}/N_{\mathrm{bulk}}} \tag{2}$$

where $I_{\mathrm{SERS}}$ is the surface-enhanced Raman intensity, $N_{\mathrm{surf}}$ is the number of molecules within the enhanced field (hot spot) region of the metallic substrate contributing to the measured SERS signal, $I_{\mathrm{ref}}$ is the Raman intensity from the reference region, and $N_{\mathrm{bulk}}$ is the number of molecules within the excitation volume of the laser spot for the analyte on

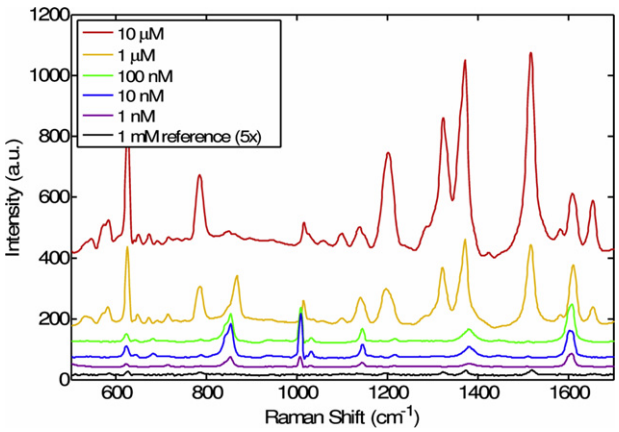


**Figure 7.** SERS spectra of R6G molecules ranging from 1 nM to 10 $\mu$M on the nanodome array substrate with $d = 17$ nm and 1 mM R6G on the reference surface without the nanodome array (the reference spectrum was multiplied by a factor of five in the plot).

the reference region. $N_{\text{bulk}}$ was calculated by the following equation

$$N_{\text{bulk}} = \pi r^2 h c N_{\text{A}} \tag{3}$$

where $r$ is the radius of the excitation laser spot (10 $\mu$m), $h$ is the thickness of the R6G spot on the reference region (0.72 $\mu$m), $c$ is the molar concentration of the R6G analyte on the reference region (1 mM), and $N_{\text{A}}$ is Avogadro's number. $N_{\text{surf}}$ was defined to be the number of molecules occupying the volume of the hot spot region with high enhancement of the local electric field. The volume of the hot spot region for calculation of $N_{\text{surf}}$ was determined from the FEM simulation of the electric field distribution around the nanodomes. The hot spot region was assumed to be bounded by the distance to which the exponentially decaying enhanced electric field in the hot spot region is reduced by a factor of $1/e$. The electric field amplitude plots along the $y$ and $z$ directions through the maximum were fitted to an exponential decay function to obtain the $1/e$ distance along the $y$ and $z$ directions. For the distance in the $x$ direction, the average distance between adjacent domes at $1/e$ values in the $z$ direction was used, approximating the curvature of the dome to be linear. Using the volume fraction of the hot spot and the SERS intensity from the 1370 cm$^{-1}$ peaks of 1 nM R6G on the SERS-active region and 1 mM R6G on the reference region for $I_{\text{SERS}}$ and $I_{\text{ref}}$, respectively, the SERS EF was calculated to be $1.37 \times 10^8$. The preceding calculation of enhancement factor describes only the enhancement that occurs within the region of highest electric field, and does not account for the fact that only a portion of the available surface area of the substrate is supporting an elevated electric field. To take into account the volume density of hot spots, the spatially averaged EF can also be calculated. For spatially averaged EF, all analyte molecules within the excitation laser spot volume are assumed to contribute equally to the measured SERS signal, so the volume fraction of the enhanced field region is not considered for the calculation. The spatially averaged EF, which represents an underestimation of the local EF from equation (2), provides a more practical, experimentally measured value of the SERS enhancement. The spatially averaged EF of the Ag nanodome array substrate was calculated to be $3.16 \times 10^6$.

## 6. Conclusion

In this paper, we have demonstrated a SERS substrate consisting of a closely spaced array of metal-coated dielectric nanodomes fabricated utilizing a low-cost, large-area nanoreplica molding method, in which the inter-dome spacing is precisely controlled through the thickness of $SiO_2$ and Ag thin films deposited over a replica molded array of polymer cylinders. FEM simulation was used to investigate the electromagnetic field distribution between adjacent nanodomes, where excellent agreement between the experimentally measured and simulated values for the intensity/enhancement dependence on inter-dome spacing was obtained. An experimentally measured SERS enhancement factor of $1.37 \times 10^8$ was demonstrated for the SERS substrate presented in this work. The nanoreplica molding process allows simple, low-cost fabrication of the required surface features over a large area, providing a path towards mass production of SERS substrates with high enhancement factors.

## Acknowledgments

The authors thank the staff of the Micro and Nanotechnology Laboratory and the Center for Nanoscale Chemical–Electrical–Mechanical Manufacturing Systems (Nano-CEMMS) at the University of Illinois at Urbana-Champaign. This material is based upon work supported by the National Science Foundation under Award No. DMI 0328162 and ECCS 09-24062. Any opinions, findings, and conclusions or recommendations expressed in this material are those of the author(s) and do not necessarily reflect the views of the National Science Foundation.

## References

[1] Grubisha D S, Lipert R J, Park H Y, Driskell J and Porter M D 2003 Femtomolar detection of prostate-specific antigen: an immunoassay based on surface-enhanced Raman scattering and immunogold labels *Anal. Chem.* **75** 5936–43

[2] Cao Y W C, Jin R C and Mirkin C A 2002 Nanoparticles with Raman spectroscopic fingerprints for DNA and RNA detection *Science* **297** 1536–40

[3] Neumann O, Zhang D M, Tam F, Lal S, Wittung-Stafshede P and Halas N J 2009 Direct optical detection of aptamer conformational changes induced by target molecules *Anal. Chem.* **81** 10002–6

[4] Shanmukh S, Jones L, Driskell J, Zhao Y P, Dluhy R and Tripp R A 2006 Rapid and sensitive detection of respiratory virus molecular signatures using a silver nanorod array SERS substrate *Nano Lett.* **6** 2630–6

[5] Jarvis R M and Goodacre R 2004 Discrimination of bacteria using surface-enhanced Raman spectroscopy *Anal. Chem.* **76** 40–7

[6] Primera-Pedrozo O M, Jerez-Rozo J I, De la Cruz-Montoya E, Luna-Pineda T, Pacheco-Londono L C and Hernandez-Rivera S P 2008 Nanotechnology-based detection of explosives and biological agents simulants *IEEE Sensors J.* **8** 963–73

[7] Fleischmann M, Hendra P J and McQuillan A J 1974 Raman-spectra of pyridine adsorbed at a silver electrode *Chem. Phys. Lett.* **26** 163–6

[8] Jeanmaire D L and Vanduyne R P 1977 Surface Raman spectroelectrochemistry.1. Heterocyclic, aromatic, and aliphatic-amines adsorbed on anodized silver electrode *J. Electroanal. Chem.* **84** 1–20

[9] Moskovits M 1985 Surface-enhanced spectroscopy *Rev. Mod. Phys.* **57** 783–826

[10] Kneipp K, Wang Y, Kneipp H, Perelman L T, Itzkan I, Dasari R and Feld M S 1997 Single molecule detection using surface-enhanced Raman scattering (SERS) *Phys. Rev. Lett.* **78** 1667–70

[11] Nie S M and Emory S R 1997 Probing single molecules and single nanoparticles by surface-enhanced Raman scattering *Science* **275** 1102–6

[12] Lu Y, Liu G L, Kim J, Mejia Y X and Lee L P 2005 Nanophotonic crescent moon structures with sharp edge for ultrasensitive biomolecular detection by local electromagnetic field enhancement effect *Nano Lett.* **5** 119–24

[13] Etchegoin P G and Le Ru E C 2008 A perspective on single molecule SERS: current status and future challenges *Phys. Chem. Chem. Phys.* **10** 6079–89

[14] Pieczonka N P W and Aroca R F 2008 Single molecule analysis by surfaced-enhanced Raman scattering *Chem. Soc. Rev.* **37** 946–54

[15] Liao P F, Bergman J G, Chemla D S, Wokaun A, Melngailis J, Hawryluk A M and Economou N P 1981 Surface-enhanced Raman-scattering from microlithographic silver particle surfaces *Chem. Phys. Lett.* **82** 355–9

[16] Gunnarsson L, Bjerneld E J, Xu H, Petronis S, Kasemo B and Kall M 2001 Interparticle coupling effects in nanofabricated substrates for surface-enhanced Raman scattering *Appl. Phys. Lett.* **78** 802–4

[17] Felidj N, Aubard J, Levi G, Krenn J R, Hohenau A, Schider G, Leitner A and Aussenegg F R 2003 Optimized surface-enhanced Raman scattering on gold nanoparticle arrays *Appl. Phys. Lett.* **82** 3095–7

[18] Felidj N, Truong S L, Aubard J, Levi G, Krenn J R, Hohenau A, Leitner A and Aussenegg F R 2004 Gold particle interaction in regular arrays probed by surface enhanced Raman scattering *J. Chem. Phys.* **120** 7141–6

[19] Gopinath A, Boriskina S V, Premasiri W R, Ziegler L, Reinhard B M and Dal Negro L 2009 Plasmonic nanogalaxies: multiscale aperiodic arrays for surface-enhanced Raman sensing *Nano Lett.* **9** 3922–9

[20] Liu G L and Lee L P 2005 Nanowell surface enhanced Raman scattering arrays fabricated by soft-lithography for label-free biomolecular detections in integrated microfluidics *Appl. Phys. Lett.* **87** 07401

[21] Baca A J, Truong T T, Cambrea L R, Montgomery J M, Gray S K, Abdula D, Banks T R, Yao J M, Nuzzo R G and Rogers J A 2009 Molded plasmonic crystals for detecting and spatially imaging surface bound species by surface-enhanced Raman scattering *Appl. Phys. Lett.* **94** 243109

[22] Haynes C L and Van Duyne R P 2001 Nanosphere lithography: a versatile nanofabrication tool for studies of size-dependent nanoparticle optics *J. Phys. Chem.* B **105** 5599–611

[23] Dick L A, McFarland A D, Haynes C L and Van Duyne R P 2002 Metal film over nanosphere (MFON) electrodes for surface-enhanced Raman spectroscopy (SERS): improvements in surface nanostructure stability and suppression of irreversible loss *J. Phys. Chem.* B **106** 853–60

[24] Gaponenko S V, Gaiduk A A, Kulakovich O S, Maskevich S A, Strekal N D, Prokhorov O A and Shelekhina V M 2001 Raman scattering enhancement using crystallographic surface of a colloidal crystal *JETP Lett.* **74** 309–11

[25] Haes A J, Haynes C L, McFarland A D, Schatz G C, Van Duyne R R and Zou S L 2005 Plasmonic materials for surface-enhanced sensing and spectroscopy *MRS Bull.* **30** 368–75

[26] Biggs K B, Camden J P, Anker J N and Van Duyne R P 2009 Surface-enhanced Raman spectroscopy of benzenethiol adsorbed from the gas phase onto silver film over nanosphere surfaces: determination of the sticking probability and detection limit time *J. Phys. Chem.* A **113** 4581–6

[27] Cunningham B T, Li P, Schulz S, Lin B, Baird C, Gerstenmaier J, Genick C, Wang F, Fine E and Laing L 2004 Label-free assays on the BIND system *J. Biomol. Screen.* **9** 481–90

[28] Block I D, Mathias P C, Ganesh N, Jones S I, Dorvel B R, Chaudhery V, Vodkin L O, Bashir R and Cunningham B T 2009 A detection instrument for enhanced-fluorescence and label-free imaging on photonic crystal surfaces *Opt. Express* **17** 13222–35

[29] Pineda M F, Chan L L Y, Kuhlenschmidt T, Choi C J, Kuhlenschmidt M and Cunningham B T 2009 Rapid specific and label-free detection of porcine rotavirus using photonic crystal biosensors *IEEE Sensors J.* **9** 470–7

[30] Ganesh N, Zhang W, Mathias P C, Chow E, Soares J A N T, Malyarchuk V, Smith A D and Cunningham B T 2007 Enhanced fluorescence emission from quantum dots on a photonic crystal surface *Nat. Nanotechnol.* **2** 515–20

[31] Zhang W, Ganesh N, Mathias P C and Cunningham B T 2008 Enhanced fluorescence on a photonic crystal surface incorporating nanorod structures *Small* **4** 2199–203

[32] Lu M, Choi S, Wagner C J, Eden J G and Cunningham B T 2008 Label free biosensor incorporating a replica-molded, vertically emitting distributed feedback laser *Appl. Phys. Lett.* **92** 261502

[33] Yang F Y, Yen G, Rasigade G, Soares J A N T and Cunningham B T 2008 Optically tuned resonant optical reflectance filter *Appl. Phys. Lett.* **92** 091115

[34] Slavik G J, Ragetly G, Ganesh N, Griffon D J and Cunningham B T 2007 A replica molding technique for producing fibrous chitosan scaffolds for cartilage engineering *J. Mater. Chem.* **17** 4095–101

[35] Lu M, Park S J, Cunningham B T and Eden J G 2007 Microcavity plasma devices and arrays fabricated by plastic-based replica molding *J. Microelectromech. Syst.* **16** 1397–402

[36] Choi C J, Block I D, Bole B, Dralle D and Cunningham B T 2009 Label-free photonic crystal biosensor integrated microfluidic chip for determination of kinetic reaction rate constants *IEEE Sensors J.* **9** 1697–704

[37] Choi C J and Cunningham B T 2006 Single-step fabrication and characterization of photonic crystal biosensors with polymer microfluidic channels *Lab Chip* **6** 1373–80

[38] Choi C J and Cunningham B T 2007 A 96-well microplate incorporating a replica molded microfluidic network integrated with photonic crystal biosensors for high throughput kinetic biomolecular interaction analysis *Lab Chip* **7** 550–6

[39] Campion A and Kambhampati P 1998 Surface-enhanced Raman scattering *Chem. Soc. Rev.* **27** 241–50

[40] Gaponenko S V and Guzatov D V 2009 Possible rationale for ultimate enhancement factor in single molecule Raman spectroscopy *Chem. Phys. Lett.* **477** 411–4

[41] Zhao Y P, Chaney S B, Shanmukh S and Dluhy R A 2006 Polarized surface enhanced raman and absorbance spectra of aligned silver nanorod arrays *J. Phys. Chem.* B **110** 3153–7

[42] Stiles P L, Dieringer J A, Shah N C and Van Duyne R R 2008 Surface-enhanced Raman spectroscopy *Annu. Rev. Anal. Chem.* **1** 601–26

[43] Zhao J, Lui H, McLean D I and Zeng H 2007 Automated autofluorescence background subtraction algorithm for biomedical Raman spectroscopy *Appl. Spectrosc.* **61** 1225–32